⌘ *Author's Choice*

THE JOURNAL OF BIOLOGICAL CHEMISTRY VOL. 286, NO. 3, pp. 2067–2077, January 21, 2011

Characterization of the Elongation Complex of Dengue Virus RNA Polymerase

ASSEMBLY, KINETICS OF NUCLEOTIDE INCORPORATION, AND FIDELITY[S]

Received for publication, July 10, 2010, and in revised form, October 30, 2010 Published, JBC Papers in Press, November 15, 2010, DOI 10.1074/jbc.M110.162685

Zhinan Jin[‡1], **Jerome Deval**[‡], **Kenneth A. Johnson**[§], **and David C. Swinney**[‡2]

From the [‡]*Virology DTA, Roche Palo Alto LLC, Palo Alto, California 94034 and the* [§]*Department of Chemistry and Biochemistry, The University of Texas, Austin, Texas 78712*

Dengue virus (DENV) infects 50–100 million people worldwide per year, causing severe public health problems. DENV RNA-dependent RNA polymerase, an attractive target for drug development, catalyzes *de novo* replication of the viral genome in three phases: initiation, transition, and elongation. The aim of this work was to characterize the mechanism of nucleotide addition catalyzed by the polymerase domain of DENV serotype 2 during elongation using transient kinetic methods. We measured the kinetics of formation of the elongation complex containing the polymerase and a double-stranded RNA by preincubation experiments. The elongation complex assembly is slow, following a one-step binding mechanism with an association rate of 0.0016 ± 0.0001 $\mu M^{-1}s^{-1}$ and a dissociation rate of 0.00020 ± 0.00005 s^{-1} at 37 °C. The elongation complex assembly is 6 times slower at 30 °C and requires Mg^{2+} during preincubation. The assembled elongation complex incorporates a correct nucleotide, GTP, to the primer with a K_d of 275 ± 52 μM and k_{pol} of 18 ± 1 s^{-1}. The fidelity of the polymerase is 1/34,000, 1/59,000, 1/135,000 for misincorporation of UTP, ATP, and CTP opposite CMP in the template, respectively. The fidelity of DENV polymerase is comparable with HIV reverse transcriptase and the poliovirus polymerase. This work reports the first description of presteady-state kinetics and fidelity for an RNA-dependent RNA polymerase from the Flaviviridae family.

Dengue virus (DENV)[3] infects 50–100 million people worldwide per year. It causes dengue fever sometimes followed by hemorrhage, shock syndrome, and death (1). DENV belongs to the Flaviviridae virus family, which includes other important human and animal pathogens such as hepatitis C virus (HCV), West Nile virus, yellow fever virus, and bovine diarrhea virus. So far there is no effective vaccine or therapeutic treatment for DENV infection. The dengue virus RNA-dependent RNA polymerase (RdRp) is a potential drug target because it replicates the viral genome (2–4). There are no approved medicines that specifically target RdRps, although HCV RdRp inhibitors are currently under clinical investigation (5). The discovery of medicines that inhibit RdRp activity is facilitated by a further understanding of the molecular basis of RdRp function and inhibition. To this end the crystal structure of RdRp domain within the NS5 protein from DENV serotype 3 was recently solved; however, a detailed kinetic analysis has yet to be reported (6).

NS5 is the largest DENV protein, about 900 amino acids in length. It contains a C-terminal RdRp domain and an N-terminal 5′-RNA methyltransferase domain (6). The recombinant full-length NS5 and its truncated RdRp domain alone, NS5pol, both can catalyze RNA replication *in vitro* (7, 8). Like other Flaviviridae polymerases, DENV RdRp carries out *de novo* RNA replication *in vivo*, meaning synthesis of the complementary RNA from the 3′ end of the template RNA without a primer (9–12). DENV RNA synthesis *in vivo* requires interactions between the polymerase, the genomic RNA, other viral proteins, and host factors (13, 14). Based on *in vitro* biochemical and structural studies, *de novo* RNA replication catalyzed by a Flaviviridae RdRp can be divided into three stages: *de novo* initiation, initiation-to-elongation transition, and elongation (7, 12, 15). During *de novo* initiation and the transition, RNA synthesis is slow and abortive, leading to accumulation of short RNA products; in contrast, RNA synthesis during elongation is thought to be relatively rapid and processive (7, 15–17). In this study we sought to develop a method to form an active elongation complex that would enable us to study the mechanism of nucleotide addition catalyzed by DENV RdRp during elongation by using transient kinetic methods.

No detailed mechanistic information of the nucleotide addition reaction catalyzed by DENV RdRp has been reported in previous *in vitro* studies (8–11). One of the limitations to these studies was that the enzymatic reactions were carried out under conditions where replication complex assembly and initiation were likely to be rate-limiting. Detailed transient kinetic studies of nucleotide addition require stoichiometric binding of RNA primer and template at the active site of the polymerase before the addition of the next incoming nucleotide. However, the assembly of a productive elongation complex containing polymerase-primer- template has been unsuccessful for RdRps from the Flaviviridae family, which in turn prevented detailed kinetic analysis of these medically

⌘ *Author's Choice*—Final version full access.

[S] The on-line version of this article (available at http://www.jbc.org) contains supplemental Fig. 1.

[1] Supported by a Roche Postdoc fellowship.

[2] To whom correspondence should be addressed: iRND3, Institute for Rare and Neglected Diseases Drug Discovery, 1514 Ridge Rd, Belmont, CA 94002. Tel.: 650-995-4270; E-mail: david.swinney@iRND3.org.

[3] The abbreviations used are: DENV, dengue virus; HCV, hepatitis C virus; RdRp, RNA-dependent RNA polymerase; CHAPS, 3-[(3-cholamidopropyl)dimethylammonio]-1-propanesulfonic acid.

important polymerases. For example, low active site concentrations of enzyme and the inability of the native enzyme to bind a double-stranded RNA (dsRNA) have limited kinetic analysis of HCV polymerase (18, 19). These limitations have been attributed to the encircled active site of Flaviviridae polymerases, which appear to only accommodate a single-stranded RNA (ssRNA) based on their crystal structures (6, 12, 20–22). However, Padmanabhan and Ackermann (10) found that higher temperature may turn DENV polymerase to an open state to allow the enzyme to bind double-stranded RNA to form an elongation complex.

In this study the assembly of the elongation complex of DENV polymerase was achieved by preincubation of NS5pol from DENV serotype 2 (DENV-2) and a primer-template RNA (P_{12}/T_{26}) at 37 °C in the presence of Mg^{2+}. We found the assembly of the productive elongation complex was stringently affected by temperature, metal ions, and enzyme concentration. Using the preassembled elongation complex, the presteady-state kinetics of nucleotide incorporation and the specificity of NS5pol were measured. The methodology developed in this study will facilitate mechanistic analysis of nucleotide addition catalyzed by DENV RdRp during elongation. Moreover, the methodology established for DENV RdRp may also apply to other Flaviviridae polymerases, thus, facilitating kinetic characterization of polymerases from this medically important virus family.

EXPERIMENTAL PROCEDURES

Chemicals and Nucleic Acids—All NTPs were ultrapure grade purchased from United States Biochemical Corp. (Cleveland, OH). Heparin sodium salt (195.9 USP units/mg) was from Sigma. $MgCl_2$, EDTA, NaCl solutions, and Tris-Cl buffers were purchased from Ambion (Austin, TX).

Unless otherwise stated (Table 1), the following RNA oligonucleotides were used in this study: 5′-GGAGAGAAAAGG-3′ (P_{12}, primer) and 5′-ACAGUUUUUUUUGCCCUUUUCUCUCC-3′ (T_{26}, template). The underlined base shows the template base for the next nucleotide incorporation. All RNA oligonucleotides were chemically synthesized and HPLC-purified by Integrated DNA Technologies, Inc. (Coralville, IA). The 5′ end labeling reaction of the P_{12} primer was conducted with [γ-^{32}P]ATP (PerkinElmer Life Sciences) and T4 polynucleotide kinase according to the manufacturer's recommendation (Invitrogen). Radiolabeled primer was purified with G25 spin columns (GE Healthcare). The recovery of the purified RNA oligonucleotides was quantified by PAGE analysis. To make the double-stranded RNA substrate, P_{12}/T_{26}, the primer, and the template were mixed at a ratio of 1: 1.1, heated at 95 °C for 2 min, and then cooled down slowly to room temperature. The P_{12}/T_{26} has 12 stable base pairs with a T_m of 54 °C calculated by the OligoAnalyzer 3.1 web application from the website of Integrated DNA Technologies, Inc. (Coralville, IA).

Expression and Purification of NS5pol—The codon-optimized cDNA sequence of DENV-2 NGC strain RdRp domain, NS5pol (residues 272–900 of NS5, starting from residues PNLDII…), was chemically synthesized by DNA2.0 Inc. (Menlo Park, CA). NS5pol was subcloned to a modified Novagen pET11a vector (EMD, Gibbstown, NJ) containing six histidine and three alanine codons in-frame at the 5′ end of the cloning site. Recombinant NS5pol was produced in BL21 Star (DE3) *Escherichia coli* cells (Invitrogen). Cells were cultured in LB medium with 100 μg/ml ampicillin at 37 °C. After the optical density reached 0.8, flasks with cells were transferred to a 4 °C cold room for 3 h. NS5pol expression was induced with 0.25 mM isopropyl 1-thio-β-D-galactopyranoside for 16 h at room temperature (25 °C). Cell pellets were collected by centrifugation at 6000 rpm for 20 min, and then the pellets were stored in a −80 °C freezer. Cell pellets were resuspended in the lysis buffer (50 mM HEPES, pH 7.0, 10% glycerol, 500 mM NaCl, 0.1% CHAPS, 1 mM DTT, and 10 mM imidazole) with the addition of 0.5 mg/ml lysozyme, 200 unit/ml Novagen Benzonase nuclease HC (purity >99%, EMD, Gibbstown, NJ), and 0.05 tablet/ml protease inhibitor mixture tablet (Roche Diagnostics). The cell lysate was sonicated and then clarified by centrifugation at 16,000 × *g* for 30 min. The supernatant was incubated with nickel-Sepharose beads (GE Healthcare) with gentle rocking at 4 °C for 1 h. The beads were loaded on a column and washed with the lysis buffer containing 50 mM imidazole. The protein was eluted with the lysis buffer containing 500 mM imidazole. The elution was diluted 5-fold with the size exclusion column buffer (SEC buffer: 25 mM HEPES, pH 7.0, 200 mM NaCl, 0.1% CHAPS, 2 mM DTT, 10% glycerol) and then concentrated to 1∼2 ml using an Amicon Ultra-15 filtration device with 30,000 nominal molecular weight limit (Millipore, Billerica, MA). The concentrated sample was loaded onto a Hiload 16/60 Superdex 75 column (GE Healthcare) and eluted with the SEC buffer. The identity of NS5pol was confirmed by mass spectrometry analysis of intact protein and tryptic-digested products.

The active site concentration of NS5pol was determined by a burst kinetic assay (supplemental Fig. 1) and was used for all the experiments in this study. The active site concentration was about 15% of the protein concentration measured by UV280 absorbance with the extinction coefficient of 170850 $cm^{-1}M^{-1}$.

Single Nucleotide Primer Extension Assay without Enzyme-RNA Preincubation—The 100-μl reaction containing NS5pol (0.6 μM), P_{12}/T_{26} (0.5 μM), and GTP (500 μM) in the reaction buffer (40 mM Tris-Cl, pH 7.4, 23.8 mM NaCl, 3 mM DTT, 15% glycerol, and 2 mM $MgCl_2$) was conducted at 37 °C. The buffer pH, NaCl, and glycerol concentrations in the reaction buffer were chosen from optimized conditions (data not shown). The same reaction buffer was used in this report unless otherwise stated. The reaction was started by the addition of NS5pol. At each time point an aliquot (5 μl) from the reaction was mixed with 15 μl of the quench solution (90% formamide, 50 mM EDTA, 0.1% bromphenol blue, and 0.1% xylene cyanol) to stop the reaction in the aliquot (Fig. 2, *B* and *C*).

Single Nucleotide Primer Extension Assay with Enzyme-RNA Preincubation—A typical preincubation reaction (100 μl) was started by mixing P_{12}/T_{26} (0.5 μM) with NS5pol (concentrations are indicated in the figure legends) in the reaction buffer at 30 or 37 °C. At each time point an aliquot (5 μl) from the preincubation reaction was immediately mixed with an

equal volume of a solution containing 1 mM GTP and 0.1 mg/ml heparin in the reaction buffer to start the single nucleotide primer extension reaction. The primer extension reaction was quenched after 90 s by mixing with 30 μl of the quench solution. Heparin was added to trap free NS5pol to ensure that the 13-mer product was generated only from the enzyme-RNA elongation complex formed during preincubation. Therefore, assaying the 13-mer product allows quantification of the formation of the elongation complex.

Mg^{2+}-dependent Elongation Complex Formation—NS5pol (0.6 μM) and P_{12}/T_{26} (0.5 μM) in the reaction buffer with $MgCl_2$ at various concentrations (0, 0.5, 1, 2, 3, 4, 5, 6 mM) were incubated at 37 °C for 1 h. The primer extension reaction was started by mixing each preincubated sample with an equal volume of a solution containing 1 mM GTP and 0.1 mg/ml heparin in the reaction buffer with $MgCl_2$ at various concentrations (4, 0.5, 1, 2, 3, 4, 5, 6 mM). The final $MgCl_2$ concentrations in the primer extension reactions were 2, 0.5, 1, 2, 3, 4, 5, and 6 mM after mixing. The reactions were quenched after 90 s. The 13-mer product represents the elongation complex formed during 1 h of incubation.

Quench-flow Assays—These assays were carried out at 37 °C using an RQF-3 chemical-quench-flow instrument (KinTek Corp., Austin, TX). In a typical quench-flow assay, a mixture of NS5pol and P_{12}/T_{26} in the reaction buffer was incubated at 37 °C for 1 h. Then the mixture was stored at room temperature during the experiment. The primer extension reaction was started by mixing each aliquot from the preincubated mixture with an equal volume of a solution containing GTP in the reaction buffer. Each reaction was quenched at a time interval indicated in the figures.

Single Nucleotide and Multiple Nucleotide Incorporation to Elongation Complexes—Each RNA substrate used in this assay had a same P_{12} primer and a T_{26} template with a different template base for the next incoming nucleotide as shown in Fig. 5 and Table 1. NS5pol (0.6 μM) and P_{12}/T_{26} (0.5 μM) in the reaction buffer were incubated at 37 °C for 1 h. Then an equal volume was added of a solution containing one correct nucleotide at 0.5 mM or all four nucleotides (each nucleotide is 0.5 mM) and 0.1 mg/ml heparin in the reaction buffer. The reactions were quenched after 90 s.

Misincorporation of Nucleotides Opposite Template CMP—Because the reactions were slow, these assays were carried out at 37 °C by hand mixing. NS5pol (0.6 μM) and P_{12}/T_{26} (0.5 μM) in the reaction buffer were incubated at 37 °C for 1 h. Primer extension reactions were initiated by mixing the assembled elongation complex with an equal volume of a solution containing NTP at various concentrations and 0.1 mg/ml heparin in the reaction buffer. Heparin was added in the nucleotide solution to prevent the complication of NS5pol and P_{12}/T_{26} rebinding. Aliquots from the reactions were mixed with the quench solution at various time intervals.

Product Analysis—The quenched reactions were heat-denatured for 3 min at 95 °C before electrophoresis. The samples were loaded onto a 16% denaturing polyacrylamide gel with 7 M urea, and electrophoresis was performed at 80 watts. Gels were dried at 82 °C for 1 h with a Model-583 gel drier (Bio-Rad). Dry gels were exposed to storage phosphor screens and visualized by using a Typhoon 9400 scanner (GE Healthcare). The intensity of the 5′ end-labeled substrates and products was quantitated by the ImageQuant software (Version 5.2, GE Healthcare).

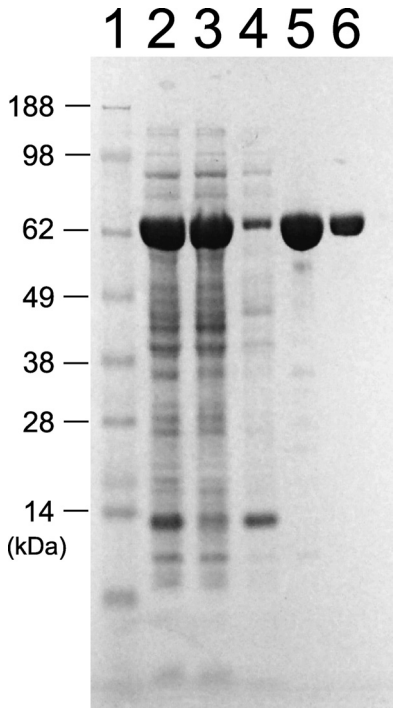

FIGURE 1. **Expression and purification of NS5pol from DENV serotype 2.** *Lanes 1–6*, marker, total cell lysate, cell pellet, supernatant, elution from nickel column, elution from Superdex 75 column.

Data Analysis—Data were analyzed by nonlinear regression using the program, GraFit5 (Erithacus Software, Surrey, UK). Each data set presented in each figure was from a representative experiment of multiple experiments with similar protocols. The data from the time courses of product formation were fit to either a single exponential equation, product = $A(1 - \exp(-k_{obs}t))$, or a double exponential equation, product = $A_1(1 - \exp(k_{obs,1}t)) + A_2(1 - \exp(-k_{obs,2}t))$, where A, A_1, and A_2 are the amplitudes of product formation, and k_{obs}, $k_{obs,1}$, and $k_{obs,2}$ are the observed rate constants. The nucleotide concentration dependence of the observed rates was fit to a hyperbola, $k_{obs} = k_{pol}S/(K_d + S)$, where k_{pol} is the maximal rate of nucleotide incorporation, K_d is the equilibrium dissociation constant for ground state binding of nucleotide, and S is the concentration of nucleotide. The parameters from data-fitting were presented in the form of best-fit value ± S.E. with their respective units. The S.E. estimates were calculated by the covariance matrix during nonlinear regression using GraFit5.

RESULTS

Protein Expression and Purification—His-tagged recombinant RNA-dependent RNA polymerase domain, NS5pol (residues 272–900 of NS5), from DENV-2 NGC strain was expressed and purified as shown in Fig. 1. RNase contamination was found in the enzyme preparation when only the nickel column was used during purification, as evidenced by the degradation of the majority RNA substrates during the replica-

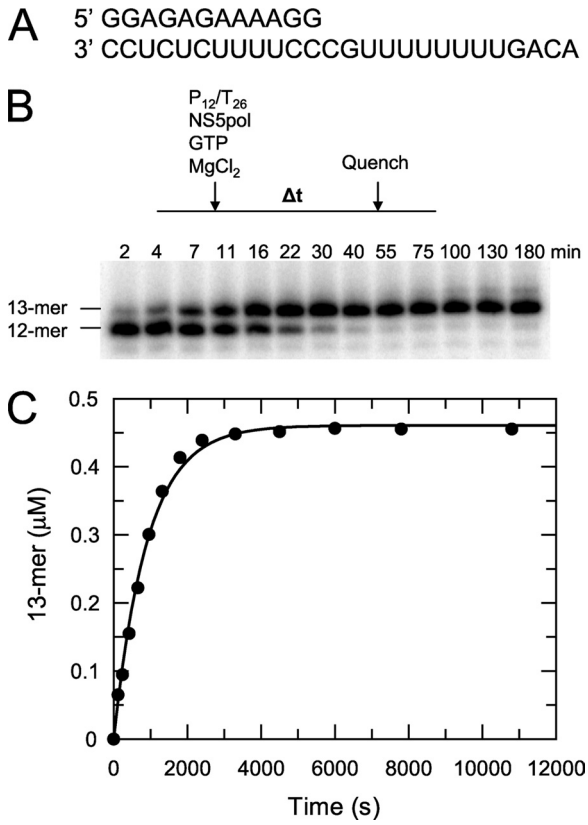

FIGURE 2. **P_{12}/T_{26} as a substrate for nucleotide incorporation catalyzed by NS5pol.** *A*, the primer/template double-stranded RNA, P_{12}/T_{26} is shown. *B*, shown is a single nucleotide primer extension assay without enzyme-RNA preincubation. The reaction was initiated at 37 °C by the addition of NS5pol (0.6 μM) to a mixture containing P_{12}/T_{26} (0.5 μM) and GTP (0.5 mM) in the reaction buffer (40 mM Tris-Cl, pH 7.4, 23.8 mM NaCl, 3 mM DTT, 15% glycerol, and 2 mM $MgCl_2$); aliquots of the reaction were quenched by a formamide-EDTA solution at the indicated times. The samples were resolved on a 16% denaturing polyacrylamide gel. *C*, shown is the time course of 13-mer product formation from the experiment described in *B*. The data were fit to a single exponential, yielding a rate of 0.00110 ± 0.00003 s^{-1} and an amplitude of 0.460 ± 0.005 μM.

tion assay (data not shown). Size-exclusion chromatography, after the nickel column, showed a small peak before a major peak. RNase contamination was found only in the small peak, and the major peak was devoid of contamination detectable during a 1-h reaction (data not shown). The major peak showed one band on an SDS gel (Fig. 1, *lane 6*) and was used as a source of enzyme for this study. The identity of the protein was confirmed by mass spectrometric analysis.

Activity of NS5pol Using a Primer/Template RNA—We designed a heteropolymeric primer/template RNA substrate (P_{12}/T_{26}) that was derived from an RNA template used in the HCV polymerase assay (Fig. 2*A*) (23). We found that NS5pol can use this P_{12}/T_{26} as a substrate by incorporating the next correct nucleotide, GTP, onto the primer. The single nucleotide primer extension reaction was initiated by the addition of NS5pol (0.6 μM) to a mixture containing P_{12}/T_{26} (0.5 μM) and GTP (0.5 mM) in the reaction buffer at 37 °C. Aliquots were removed from the reaction at various time intervals and mixed with the quench solution to stop reactions (Fig. 2, *B* and *C*). Because the assay was performed under single turnover conditions in which more NS5pol was added than P_{12}/T_{26}, the time course of 13-mer formation was fit to a single

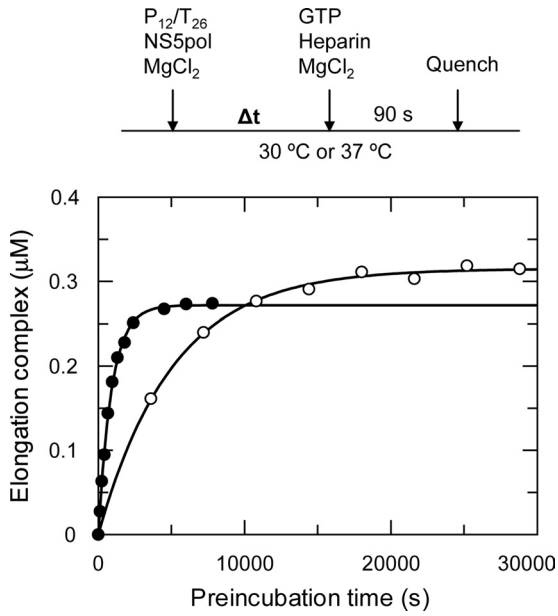

FIGURE 3. **Kinetics of elongation complex assembly at different temperatures.** The preincubation reactions were started by mixing NS5pol (0.6 μM) and P_{12}/T_{26} (0.5 μM) in the reaction buffer at 30 °C (*open circles*) and 37 °C (*close circles*). The elongation complexes assembled during preincubation were quantified by single nucleotide primer extension reaction (see "Experimental Procedures"). Each time course of elongation complex formation was fit to a single exponential equation, yielding a rate of 0.00110 ± 0.00003 s^{-1} with an amplitude of 0.270 ± 0.002 μM for reactions at 37 °C and a rate of 0.00020 ± 0.00007 s^{-1} with an amplitude of 0.320 ± 0.003 μM for reactions at 30 °C.

exponential, yielding a k_{obs} of 0.00110 ± 0.00003 s^{-1} with an amplitude of 0.46 ± 0.005 μM. Although 92% of the RNA reacted to form product in this assay, the rate of one nucleotide incorporation, with a half-life of 10 min, was too slow to represent the rate of nucleotide incorporation during elongation *in vivo*.

Time-dependent Formation of the Elongation Complex—We hypothesized that the slow rate was due to the slow formation of the elongation complex, NS5pol-primer-template. Therefore, we studied the formation of the elongation complex by preincubation of NS5pol (0.6 μM) and P_{12}/T_{26} (0.5 μM) for specific time intervals before the addition of GTP. The study was performed at two different temperatures: 30 and 37 °C (Fig. 3). After preincubation for various time intervals, aliquots from the mixture were rapidly mixed with 0.5 mM GTP to initiate the single nucleotide incorporation reactions, and the reactions were quenched after 90 s. We chose a 90-s reaction time because the burst phase of 13-mer product formation during elongation was completed in this time interval (see below). Heparin was added with the GTP solution to trap free NS5pol to ensure that the 13-mer was generated only from the elongation complex formed during preincubation. Accordingly, the concentration of the 13-mer product formed will equal the concentration of the elongation complex formed during the preincubation phase. The time course of preincubation to form the elongation complex at 37 °C was fit to a single exponential, yielding a rate of 0.00110 ± 0.00003 s^{-1} ($t_{½}$ = 10.5 min) and an amplitude of 0.270 ± 0.002 μM; at 30 °C, the rate was 0.00020 ± 0.00007 s^{-1} ($t_{½}$ = 58 min), and the amplitude was 0.320 ± 0.003 μM. The rate of elongation

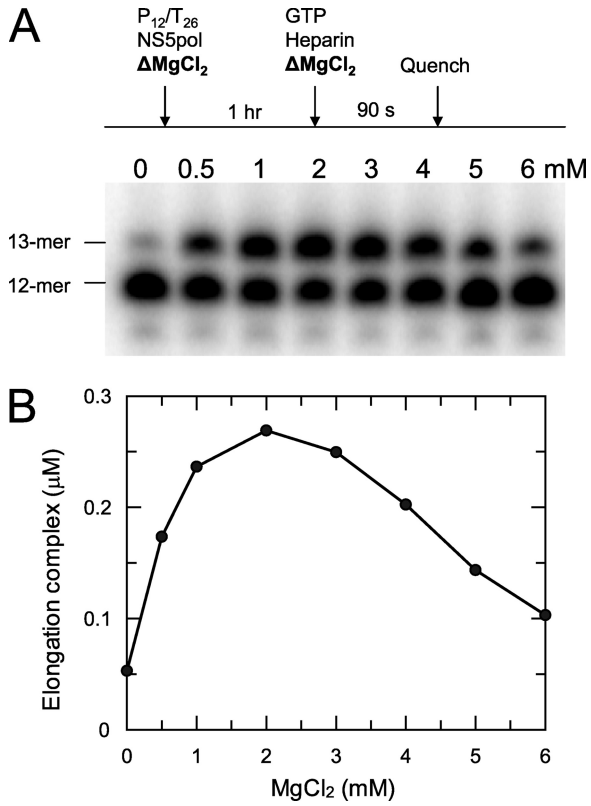

FIGURE 4. **Mg^{2+}-dependent formation of the elongation complex.** NS5pol (0.6 μM) and P_{12}/T_{26} (0.5 μM) were preincubated at 37 °C in the reaction buffer with $MgCl_2$ at various concentrations (0, 0.5, 1, 2, 3, 4, 5, 6 mM) for 1 h. The elongation complexes formed during 1 h of preincubation were quantified by primer extension reaction. Each preincubated sample was mixed with an equal volume of a solution containing 1 mM GTP and 0.1 mg/ml heparin in the reaction buffer with $MgCl_2$ at various concentrations (4, 0.5, 1, 2, 3, 4, 5, 6 mM) to start the primer extension reaction. The reactions were quenched after 90 s and analyzed by PAGE. The gel image and the plot of elongation complex concentration *versus* $MgCl_2$ concentration are shown in *A* and *B*, respectively.

complex formation by preincubation of NS5pol with P_{12}/T_{26} at 37 °C was identical to the rate of nucleotide incorporation without preincubation (Fig. 2*C*), strongly suggesting that the elongation complex assembly was rate-limiting. Also, the rate of elongation complex formation at 37 °C was about 6 times faster than at 30 °C. Preincubation studies at room temperature (23 °C) showed less than 0.05 μM elongation complexes were formed even after preincubation for 4 h (data not shown).

Mg^{2+}-dependent Elongation Complex Formation—Several earlier studies reported different roles for divalent metal ions in the polymerase function (24, 25). We examined the effect of $MgCl_2$ on the formation of the elongation complex (Fig. 4). In this experiment, NS5pol (0.6 μM) and P_{12}/T_{26} (0.5 μM) were preincubated with $MgCl_2$ (0–6 mM) in the reaction buffer for 1 h at 37 °C. Then primer extension reaction was initiated by the addition of GTP in the presence of $MgCl_2$ and heparin. The reactions were quenched after 90 s, and the reactions were analyzed by PAGE. The gel of the results and the plot of elongation complexes formed during 1 h of preincubation *versus* $MgCl_2$ concentration are shown in Fig. 4. The observed optimal concentration of $MgCl_2$ is around 2 mM. Surprisingly, only about 10% of total RNA (0.05 μM) was assembled into active elongation complexes after preincubation of enzyme and RNA without $MgCl_2$ (*lane 1* in Fig. 4*A* and the *first data point* in Fig. 4*B*) compared with about 55% of the RNA (0.275 μM) assembled after preincubation with 2 mM $MgCl_2$ (*lane 4* in Fig. 4*A* and the *fourth data point* in Fig. 4*B*). Both samples contained 2 mM $MgCl_2$ during the 90-s primer extension reaction. This comparison indicates that $MgCl_2$ is necessary for efficient formation of the elongation complex during preincubation. The $MgCl_2$-dependent elongation complex formation was also observed at 30 °C (data not shown).

Nucleotide Incorporation Catalyzed by NS5pol in the Elongation Complex—The rate of nucleotide incorporation from the assembled elongation complex was measured in a rapid mixing/quenching experiment. NS5pol (0.6 μM) and P_{12}/T_{26} (0.5 μM) were incubated in the reaction buffer for 1 h at 37 °C and then rapidly mixed with an equal volume of GTP solution in the reaction buffer. After mixing, the final concentrations of NS5pol, P_{12}/T_{26}, and GTP were 0.3, 0.25, and 800 μM, respectively. The reactions were quenched at various time intervals (Fig. 5*A*). The time course of 13-mer formation was fit to a two-exponential equation; the fast exponential gave a rate of $13.2 \pm 0.8\ s^{-1}$ and an amplitude of 0.083 ± 0.002 μM. The slow exponential gave a rate of $0.22 \pm 0.01\ s^{-1}$ and an amplitude of 0.094 ± 0.002 μM. This result demonstrates that nucleotide addition to the primer catalyzed by NS5pol in the assembled elongation complex is much faster than the assembly of elongation complex.

Single and multiple nucleotide incorporation reactions were examined to explore the kinetics of primer extension using the pre-assembled elongation complex (Fig. 5*B*). NS5pol and P_{12}/T_{26} were incubated for 1 h at 37 °C, and then the primer extension reactions were initiated by adding one or all four nucleotides with heparin. The reactions were quenched after 90 s. In this experiment, four different P_{12}/T_{26} RNA substrates were used; each has the same P_{12} primer but used a T_{26} template with different template bases for the next incoming nucleotide (Table 1). A rapid burst of formation of the 13-mer product was observed for all RNA substrates when only one nucleotide was added, suggesting single nucleotide incorporation from the assembled elongation complex was fast and independent of the identity of the correct base pair (Fig. 5*B*). In contrast, the majority of the products were full-length (26-mer) when all four nucleotides were included in the reaction, although a ladder of products of intermediate size was also apparent. We conclude that the 26-mer product was formed from one enzyme binding event, as heparin prevents rebinding of the enzyme to RNA after dissociation. These results suggest that incorporation of multiple nucleotides was fast and moderately processive.

Kinetic Mechanism of Elongation Complex Assembly—The time dependence of formation of the elongation complex was characterized with NS5pol at various concentrations to study the kinetic mechanism of assembly (Fig. 6). Preincubation reactions to form the elongation complex were started by mixing P_{12}/T_{26} (0.5 μM) with NS5pol at various concentrations (0.15–0.9 μM) in the reaction buffer at 37 °C. Elongation complexes formed during preincubation for an indicated time

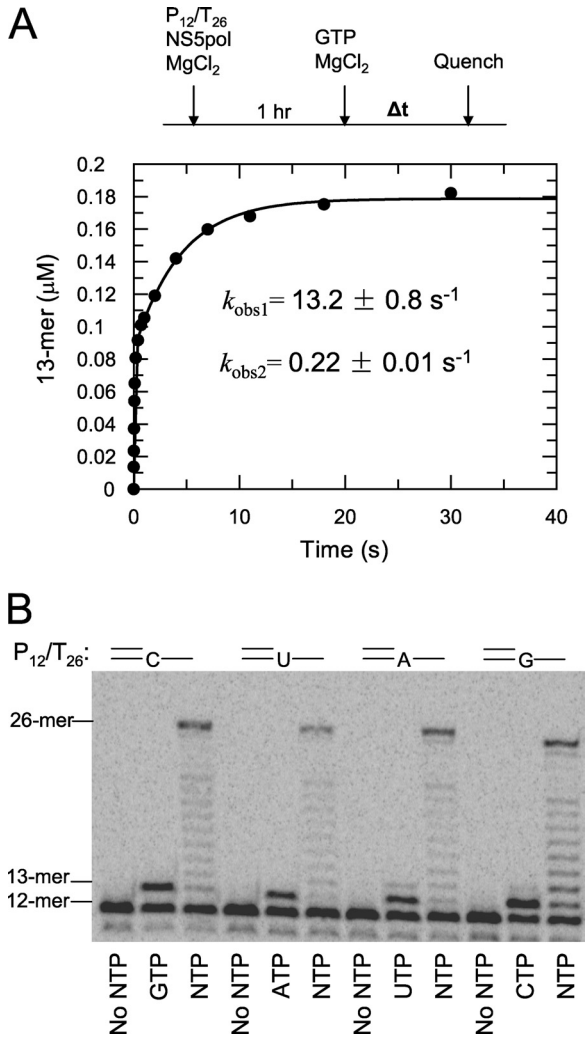

FIGURE 5. **Nucleotide incorporation catalyzed by NS5pol in the elongation complex.** *A*, kinetics of GTP incorporation are shown. NS5pol (0.6 μM) and P_{12}/T_{26} (0.5 μM) in the reaction buffer were incubated at 37 °C for 1 h. Aliquots of this mixture were rapidly mixed with GTP (0.8 mM after mixing), and then the reactions were quenched at various time intervals in a quench-flow instrument. The concentration of NS5pol and P_{12}/T_{26} after mixing was 0.3 and 0.25 μM, respectively. The time course of 13-mer formation is shown. The data were fit to a two-exponential equation; the fast exponential had a rate of 13.2 ± 0.8 s^{-1} and an amplitude of 0.083 ± 0.002 μM, and the slow exponential had a rate of 0.22 ± 0.01 s^{-1} and an amplitude of 0.094 ± 0.002 μM. *B*, shown is primer extension with a single nucleotide or all four nucleotides. After incubation of NS5pol and P_{12}/T_{26} (the template of each RNA has different template base for next incoming nucleotide, see Table 1) in the reaction buffer for 1 h at 37 °C, each preincubated sample was mixed with an equal volume of a solution containing single nucleotide at 0.5 mM or all four nucleotides (each nucleotide is 0.5 mM) and 0.1 mg/ml heparin in the reaction buffer. The reactions were quenched after 90 s and analyzed by PAGE.

TABLE 1
RNA substrates

P_{12}/T_{26}	5′-GGAGAGAAAAGG 3′-CCUCUCUUUUCCCGUUUUUUUUGACA-5′
P_{12}/T_{26_14U}	5′-GGAGAGAAAAGG 3′-CCUCUCUUUUCCUGUUUUUUUUGACA-5′
P_{12}/T_{26_14A}	5′-GGAGAGAAAAGG 3′-CCUCUCUUUUCCAGUUUUUUUUGACA-5′
P_{12}/T_{26_14G}	5′-GGAGAGAAAAGG 3′-CCUCUCUUUUCCGCUUUUUUUUGACA-5′

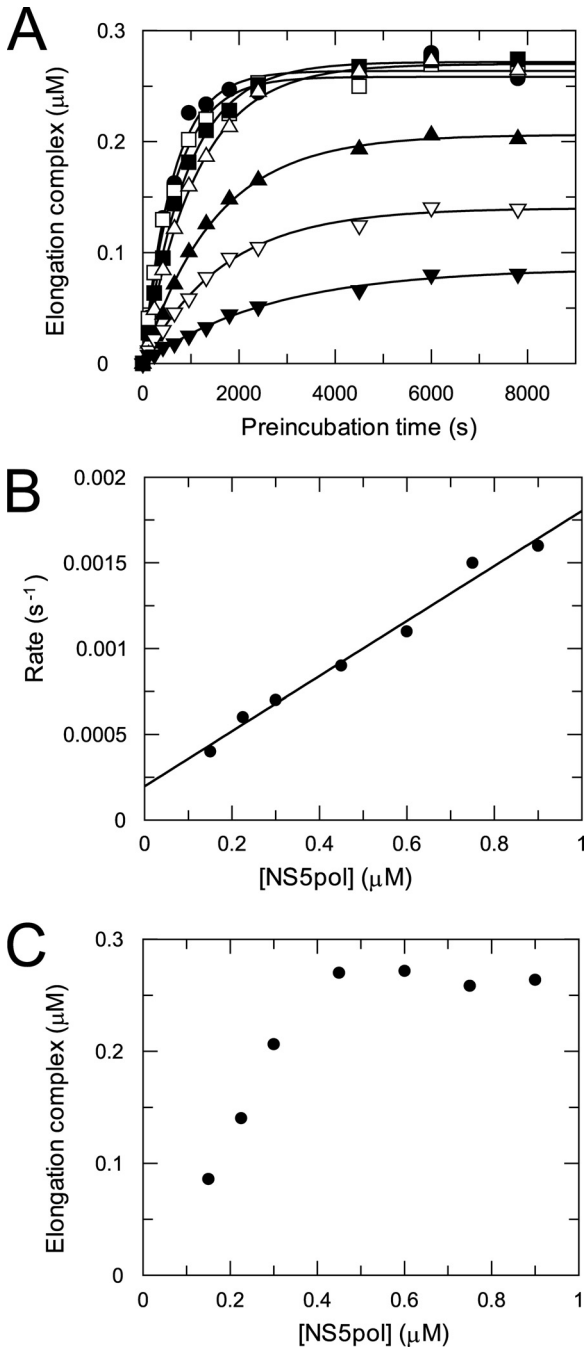

FIGURE 6. **Kinetics of elongation complex assembly with NS5pol at various concentrations.** *A*, shown are time courses of elongation complex formation at various NS5pol concentrations. Preincubation reactions were started at 37 °C by mixing P_{12}/T_{26} (0.5 μM) with NS5pol at various concentrations (0.15 (▼), 0.23 (▽), 0.3 (▲), 0.45 (▽), 0.6 (■), 0.75 (□), 0.9(●) μM) in the reaction buffer. The elongation complexes assembled during preincubation were quantified by single nucleotide primer extension reaction. Each time course of elongation complex formation was fit to a single exponential equation to obtain the observed rate of assembly and the amplitude of assembled complexes at each NS5pol concentration. The *solid lines* are the best fits. *B*, shown is the plot of the observed rate *versus* NS5pol concentration. The data were fit to a linear function, giving a slope of 0.0016 ± 0.0001 $\mu M^{-1}s^{-1}$ and an intercept of 0.00020 ± 0.00005 s^{-1}. *C*, the plot of the amplitude *versus* NS5pol concentration is shown.

interval were quantified by the amount of 13-mer product. Each time course of elongation complex formation was fit to a single exponential equation to obtain the observed rate of assembly and the amplitude of assembled elongation complexes (Fig. 6*A*). The observed rates of assembly were plotted against NS5pol concentrations (Fig. 6*B*). The data in the plot

can be fit to a linear function, giving a slope of 0.0016 ± 0.0001 $\mu M^{-1}s^{-1}$ and an intercept of 0.00020 ± 0.00005 s^{-1}. The results indicate that the binding of NS5pol and P_{12}/T_{26} to form the elongation complex follows a one-step binding mechanism with an association rate of 0.0016 ± 0.0001 $\mu M^{-1}s^{-1}$ and a dissociation rate of 0.00020 ± 0.00005 s^{-1} (Scheme 1). Based on these two rates, the estimated binding K_d of the enzyme and RNA to form the productive elongation complex is about 0.13 μM. As shown in Fig. 6*C*, the maximal amplitude of assembled elongation complexes is 0.27 μM, which is about 54% of the input RNA (0.5 μM). Assembly of the elongation complex at higher enzyme concentration (> 0.45 μM) does not increase the amplitude, suggesting only about half of the *E*-RNA complexes were able to form productive elongation complexes during preincubation. A fraction of the RNA could be bound to the enzyme nonproductively, or there could be some loss of activity during the preincubation phase. The fractional recovery of active elongation complexes is comparable with that seen with HIV reverse transcriptase (26).

Kinetics of Correct and Incorrect Nucleotide Incorporation during Elongation—The kinetics of single nucleotide incorporation from an assembled elongation complex were studied at various NTP concentrations to determine the apparent nucleotide equilibrium dissociation constant (K_d) and maximal incorporation rate (k_{pol}). The kinetics of correct single nucleotide incorporation were determined by rapidly mixing the assembled elongation complex with GTP at various concentrations in a quench-flow instrument. The time courses of product formation at various GTP concentrations are shown in Fig. 7*A*. Each time course was best fit to a two-exponential equation. The origin of the slow phase is not known; it could be due to a shift of the RNA from a nonproductive to a productive binding mode or other isomerization in the *E*-RNA complex. In any case, the rate of the fast phase describes the kinetics of the reaction of the productive *E*-RNA complex. Therefore, the rates from the fast phase were plotted against GTP concentration, and the data were fit to a hyperbola, yielding a K_d of 275 ± 52 μM and a k_{pol} of 18 ± 1 s^{-1} (Fig. 7, *B* and *C*) to define the kinetic parameters governing nucleotide incorporation.

The kinetics of misincorporation opposite CMP in the template were studied at various NTP concentrations. As an example, the time courses of product formation at various UTP concentrations are shown in Fig. 8. The data were fit to a single exponential to determine the observed rates. The rates were plotted against UTP concentrations, and the data were fit to a hyperbola to give a K_d of 1.6 ± 0.8 mM and a k_{pol} of 0.0030 ± 0.0006 s^{-1}. The kinetic parameters for correct and incorrect nucleotide incorporations opposite CMP are summarized in Table 2.

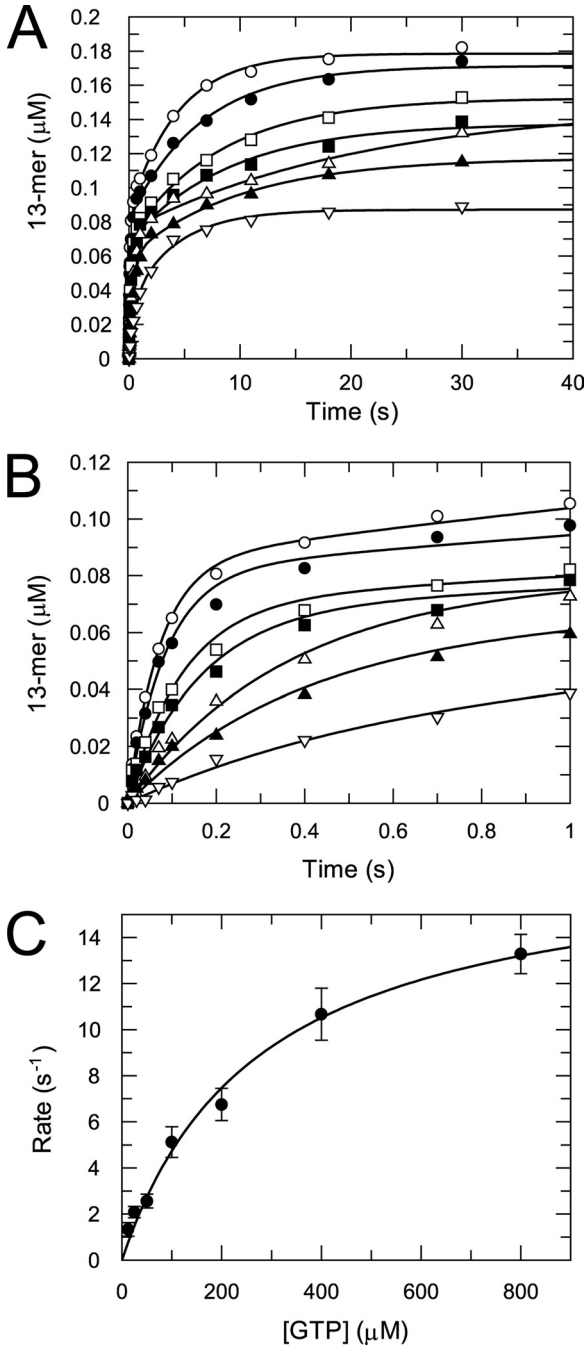

FIGURE 7. **GTP concentration dependence of the kinetics of correct nucleotide incorporation.** *A*, time courses of GTP incorporation opposite CMP in template at various GTP concentrations are shown. A mixture of NS5pol (0.6 μM) and P_{12}/T_{26} (0.5 μM) in reaction buffer were incubated at 37 °C for 1 h. Aliquots of this mixture were rapidly mixed with GTP (12.5 (▽), 25 (▲), 50 (△)100 (■), 200 (□), 400 (●), and 800 (○) μM after mixing) to start nucleotide incorporation reactions. The concentration of NS5pol and P_{12}/T_{26} after mixing is 0.3 and 0.25 μM, respectively. The reactions were quenched at various time intervals. Each time course was fit to a two-exponential equation (*solid lines*). *B*, data within 1-s reaction time from *A* are shown to demonstrate the fitting of the fast phase. *C*, shown is GTP concentration dependence of the incorporation rate for the fast phase. The rates of the fast phase were plotted against GTP concentration, and the data were fit to a hyperbola, yielding a K_d of 275 ± 52 μM and a k_{pol} of 18 ± 1 s^{-1}.

DISCUSSION

RNA de novo replication undergoes three phases: initiation, initiation-to-elongation transition, and elongation (12, 27). To date no one has reported a detailed kinetic characterization of dengue virus polymerase in the elongation phase. In this work we report the conditions required for assembly of the elongation complex of DENV RdRp using a double-stranded RNA substrate, P_{12}/T_{26}, and the polymerase domain, NS5pol. The reaction of nucleotide incorporation catalyzed

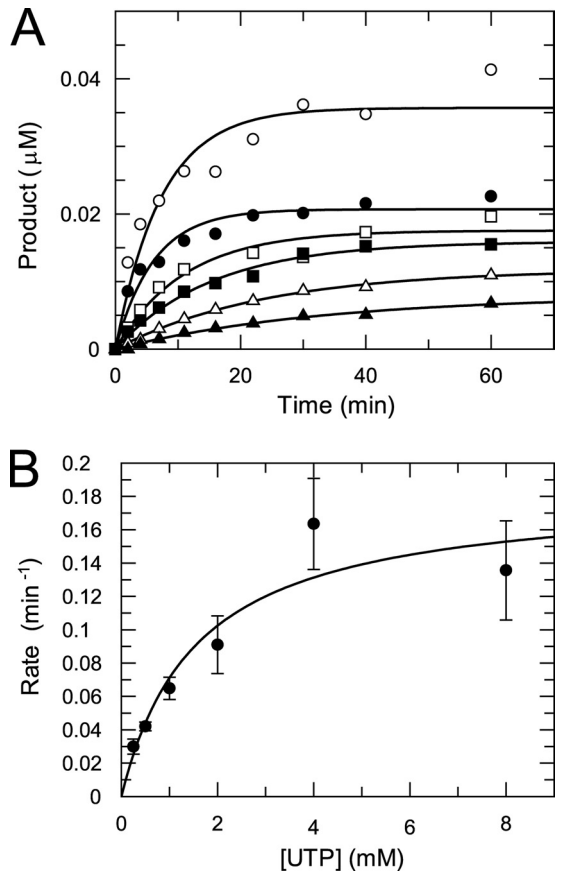

FIGURE 8. **UTP concentration dependence of the kinetics of misincorporation.** *A*, shown are time courses of UTP misincorporation at various UTP concentrations. A mixture of NS5pol (0.6 μM) and P_{12}/T_{26} (0.5 μM) in the reaction buffer was incubated at 37 °C for 1 h. Then the nucleotide incorporation reactions were initiated by adding an equal volume of UTP solution (0.25 (▲), 0.5 (△), 1 (■), 2 (□), 4 (●), 8 (○) mM after mixing) in the reaction buffer with heparin (0.05 mg/ml after mixing). The concentration of NS5pol and P_{12}/T_{26} after mixing was 0.3 and 0.25 μM, respectively. At various time intervals, aliquots from the reaction were removed and mixed with the quench solution. Each time course of product formation was fit to a single exponential to obtain the observed misincorporation rate. *B*, UTP concentration dependence of the misincorporation rate is shown. The observed rates were plotted against UTP concentration, and the data were fit to a hyperbola, yielding a K_d of 1.6 ± 0.8 mM and a k_{pol} of 0.0030 ± 0.0006 s^{-1}.

by NS5pol in the assembled elongation complex was characterized, leading to the minimal mechanism for formation of the elongation complex and subsequent nucleotide incorporation shown in Scheme 1.

$$\text{Assembly: } E + R_n \underset{0.0002\ s^{-1}}{\overset{0.0016\ \mu M^{-1}s^{-1}}{\rightleftharpoons}} E \cdot R_n$$

$$\text{Elongation: } E \cdot R_n + N \overset{275\ \mu M}{\rightleftharpoons} E \cdot R_n \cdot N \xrightarrow{18\ s^{-1}} E \cdot R_{n+1} + PP_i$$

SCHEME 1. **Minimal kinetic mechanism of elongation complex assembly followed by nucleotide binding and incorporation.** *E*, NS5pol; R_n, P_{12}/T_{26}; *N*, NTP; R_{n+1}, P_{13}/T_{26}; PP_i, pyrophosphate.

Assembly of the Elongation Complex—Elongation complex ($E{\cdot}R_n$) assembly from P_{12}/T_{26} and NS5pol was followed by nucleotide binding to form a ternary complex ($E{\cdot}R_n{\cdot}N$) and subsequent nucleotide incorporation. Elongation complex assembly is the slowest step in the pathway; the rate of nucleotide incorporation was 0.0011 s^{-1} without preincubation (Fig. 2) and 13.2 s^{-1} after preincubation of enzyme and RNA (Fig. 5*A*). A detailed kinetic study of the assembly shows that the binding of enzyme and RNA to form $E{\cdot}R_n$ can be described by a simple one-step binding mechanism with an association rate of 0.0016 ± 0.0001 $\mu M^{-1}s^{-1}$ and a dissociation rate of 0.00020 ± 0.00005 s^{-1} when preincubation was performed at 37 °C (Fig. 6). Based on these two rates, the apparent K_d for the formation of the $E{\cdot}R_n$ complex is about 0.13 μM. However, the exceedingly slow rate and the extreme temperature dependence (discussed below) suggest that the process of forming the elongation complex is much more complex and may require several steps. Although one expects that initial weak RNA binding may then lead to subsequent isomerization to form a productive complex, there are no data to resolve the individual steps.

TABLE 2
Kinetic constants of nucleotide incorporation opposite template CMP

NTP	k_{pol}	K_d	k_{pol}/K_d	Discrimination[a]
	s^{-1}	μM	$\mu M^{-1}s^{-1}$	
GTP	18 ± 1	275 ± 52	0.065	1
UTP	0.0030 ± 0.0006	1570 ± 820	0.0000019	34,000
ATP	0.0013 ± 0.0004	1180 ± 1000	0.0000011	59,000
CTP	0.00053 ± 0.00011	1100 ± 600	0.00000048	135,000

[a] Discrimination is the ratio of the specificity for a correct nucleotide (GTP in this case) to that of an incorrect nucleotide.

One interesting observation regarding elongation complex assembly is that the assembly rate at 37 °C is about 6 times faster than at 30 °C (Fig. 3); at room temperature the assembly rate was negligible (data not shown). This observation is similar to that of Ackermann and Padmanabhan (10), which led to the proposal that the binding of a dsRNA or a ssRNA to DENV RdRp is regulated by a temperature-dependent switch on the enzyme. They proposed that at higher temperatures the enzyme switches to an open conformational state for dsRNA to bind and form the elongation complex. The structure of the apo-form of DENV-3 NS5pol is similar to a canonical polymerase, resembling a human right hand with fingers, palm, and thumb domains (Fig. 9). Apparently, the active site of apo NS5pol is encircled by extensions from the fingers and thumb domain, leading to a narrow RNA binding channel that appears to only accommodate a ssRNA (6). The narrow RNA binding channel is conserved in several polymerases that catalyze *de novo* RNA replication (28). Although the exact structural basis for the temperature-dependent switch is unclear, evidence from structural and biochemical studies of several Flaviviridae polymerases provided possible mechanisms involving rearrangements of two different loops, one in the thumb domain (Fig. 9, *red loop*), named the priming loop in DENV, and the other connecting the fingers and thumb domains (Fig. 9, *blue loop*), named Δ1 loop-like structure (12, 29). The priming loop protrudes into the active site to prevent the binding of a dsRNA in DENV. In HCV polymerase, deletion of eight residues in the homologous β loop allows the polymerase to bind a dsRNA (19, 30). Lesburg *et al.* (20) proposed that the β loop opens to allow exit of duplex RNA product during the elongation phase and interacts with the major groove of the duplex RNA to improve replication pro-

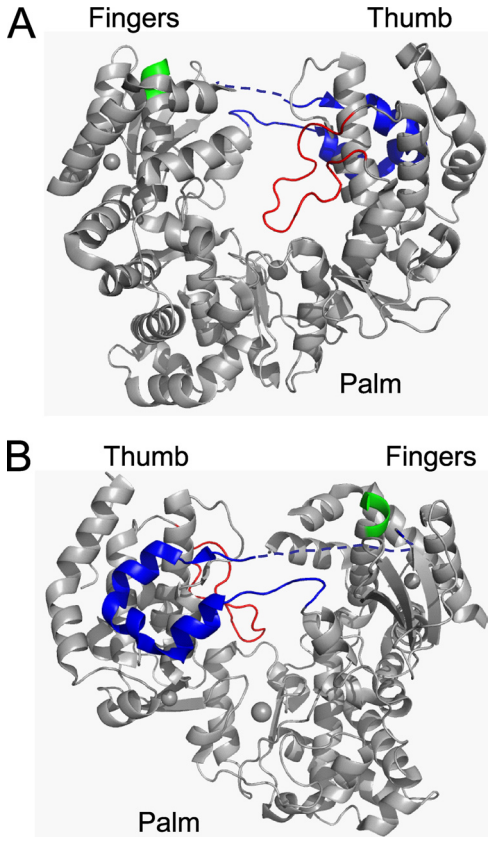

FIGURE 9. **Crystal structure of the apo-form of DENV-3 RdRp (residues 273–900).** *A*, the front view of the crystal structure resembles a human right hand with fingers, palm, and thumb domains. The RNA is assumed to occupy the space between fingers and thumb domains. The priming loop (shown in *red*) protrudes into the active site and presumably opens when dsRNA product exits the active site. Δ1 loop-like structure (in *blue*) protrudes from the fingers domain and docks on the thumb domain. The missing residues of the structure (residues 311–316) are represented by the *broken lines*. Motif F is shown in *green*. *B*, the back view of the structure is shown. Pictures were drawn from PDB file 2J7U (6).

cessivity. The β loop connects to the body of the thumb domain through two hinges. Only minor changes in the backbone torsion angles are required to allow the opening of this β loop. The movement of these loop structures is likely to be highly sensitive to temperature (31). Similarly, the binding of a dsRNA has been proposed to be controlled by a flexible locking mechanism through the Δ1 loop-like structure, which is conserved in Flaviviridae RdRps (29). We speculate that dsRNA binds to the open conformational state of the dengue polymerase through temperature-sensitive and Mg^{2+}-dependent structural rearrangements involving flexible loop movements and that higher temperature increases the frequency of the close-to-open transition of two possible loops discussed above, thus, accelerating the assembly process.

Nucleotide Incorporation Catalyzed by DENV RdRp during Elongation—DNA and RNA polymerases use a similar minimal mechanism to catalyze nucleotide incorporation; that is, ground state binding of nucleotide to form the ternary enzyme-RNA-nucleotide complex followed by incorporation of nucleotide (Scheme 1). The kinetic constants for these two steps, K_d and k_{pol}, respectively, are determined by nucleotide incorporation assay at various nucleotide concentrations. The time courses of 13-mer formation from the assembled NS5pol elongation complexes best fit to a two-exponential equation (Fig. 7). Data analysis of the fast phase yields a K_d of 275 ± 52 μM and a k_{pol} of 18 ± 1 s^{-1}, which are comparable with other well characterized RdRps (32, 33).

As stated above, the kinetics show that there are at least two distinct kinetic processes that contribute to nucleotide elongation. We have interpreted these kinetics to suggest that there are at least two different conformational states involving the elongation complex, one that catalyzes nucleotide incorporation at faster rate and one or more that can isomerize to the active form or catalyze nucleotide incorporation at a slower rate. The relationship of the slower step to the faster step is currently under investigation. Understanding the mechanistic features that contribute to the slower rate may provide further insights in the RNA binding and nucleotide incorporation mechanism. The work reported here focuses on the faster rate as it is more likely to be physiologically relevant during viral genome replication *in vivo*.

During RNA replication, a polymerase has to selectively incorporate one correct nucleotide of four available nucleotides opposite a given RNA template base. A polymerase achieves such selectivity by incorporating competing nucleotides with different specificity. The specificity constant for incorporation of each nucleotide by NS5pol is defined as k_{pol}/K_d, which is equal to k_{cat}/K_m for sequential incorporation during processive synthesis. In our study, K_d and k_{pol} for the correct and incorrect nucleotides were measured by single turnover nucleotide incorporation assays (Table 2). Based on these measurements, the specificities for all four nucleotides are in the order of G, U, A, C, from high to low specificity, for nucleotide incorporation against a CMP in the template. The discrimination against a mispair *versus* a correct base pair can be calculated by the ratio of k_{pol}/K_d for the correct to the incorrect (Table 2). For example, the discrimination of NS5pol for U:C *versus* G:C was 34,000, meaning one UTP can be misincorporated for every 34,000 template CMPs. Accordingly, the fidelity or error rate for NS5pol was between 1/34,000 for the U:C mispair and 1/135,000 for the C:C mispair.

The contribution to the observed fidelity of NS5pol from the ground state binding step is mainly due to base pairing. The ground state binding affinity of a mispair is about 4–5.7-fold weaker than the cognate G:C pair (Table 2). Therefore, the free energy difference for ground state binding ($\Delta\Delta G = -RT\ln(K_c/K_i)$; K_c and K_i are the equilibrium binding constants for correct and incorrect nucleotides, respectively) is about 0.85–1.1 kcal/mol. The free energy difference between correct and incorrect base pairs in enzyme-free conditions was estimated to be 1–3 kcal/mol (34). The similarity in the differential binding energies with and without enzyme suggests that the interaction of nucleotides with NS5pol contributes little to the selection of correct and incorrect base pairs during ground state binding. However, if a nucleotide-dependent conformational change governs the kinetics of correct nucleotide incorporation, then these calculations may not be valid (35, 36).

The K_d for the cognate G:C binding is 275 μM, which is much higher than those for replicative DNA polymerases such as human mitochondrial DNA polymerase, hPolγ, (0.8

μM) (37), T7 DNA polymerase (20 μM) (38), and HIV reverse transcriptase (1.5 μM) (36). High K_d values for correct nucleotide binding were also observed in *Sulfolobus solfataricus* DNA polymerase Dpo4 (171 μM) (39), T7 RNA polymerase (300 μM) (40), poliovirus $3D^{pol}$ (130 μM) (32), and foot-and-mouth disease virus polymerase (50–500 μM) (33). The low binding affinity has been attributed to a loose, solvent-accessible active site in Dpo4 (39, 41). In contrast, the ternary complex structure of T7 DNA polymerase has a tight active site. Our data are consistent with a loose active site for NS5pol where the amino acids make minimal interactions with the nascent base pair during ground state binding.

The difference between the rates of correct and incorrect nucleotide incorporation for NS5pol is large in contrast to the minimal discrimination at the ground state binding step. The rates of misincorporation were 6,000–34,000-fold slower than the rate for incorporating the correct nucleotide. For hPolγ and T7 DNA polymerase, incorrect nucleotides were incorporated at rates 370~12,000-fold and 2,000~4,000-fold slower than correct nucleotides, respectively (37, 38). For HIV reverse transcriptase, the difference is only 7~90-fold (36). Therefore, the nucleotide incorporation step catalyzed by NS5pol was the primary determinant of its fidelity. It is not clear how the small energy difference in base-pairing during ground state binding is translated to the larger energy difference observed in catalysis. Conformational changes exist between the ground state binding and the chemistry step for many polymerases (34). For T7 DNA polymerase, the conformational change can stabilize the binding of a correct nucleotide for fast catalysis but destabilize the binding of an incorrect nucleotide and misalign the active site for slow chemistry. It is possible that NS5pol also follows the similar mechanism adopted by T7 DNA polymerase. The motif F (Fig. 9, shown in *green*) of DENV-3 NS5pol has several conserved basic residues that were thought to provide a binding site for the incoming nucleotide during catalysis (20). However, motif F is far from the active site in the structure (Fig. 9). A major movement of motif F would be required for it to interact with a base pair in the active site. Further research is under way to address this proposal.

The observed fidelity of NS5pol was comparable with replicative DNA polymerases without their exonuclease activity, such as hPolγ (exo^-) (37, 42). The error rate of NS5pol is only 1 order of magnitude lower than that of T7 DNA polymerase (exo^-) (38). The fidelity of NS5pol is about 10-fold higher than HIV reverse transcriptase (26) and is also higher than many DNA repair polymerases such as rat DNA polymerase β and Dpo4 (39, 43). Similar fidelity was also observed with other RdRps, such as poliovirus $3D^{pol}$ and foot-and-mouth disease virus RdRp (32, 33). These comparisons assume that the fidelity we measured for NS5pol is similar across all combinations of base pairs, as seen with DNA-dependent DNA polymerases (37).

Because RNA polymerases lack the proofreading 3′-5′-exonuclease activity, which can contribute 10–100-fold to fidelity, NS5pol is still deemed to exhibit low fidelity compared with hPolγ and T7 DNA polymerase with their exonuclease activity (44, 45). In addition, most RNA viruses are deficient in error correction mechanisms; therefore, the overall mutation rates per genome replication for RNA viruses are close to the error rate of their polymerases. The fidelity measured from our assay predicts the error rate in the range of 1/34,000 to 1/135,000 for DENV-2, which is in the range of 10^{-3}–10^{-5} observed for viruses with a positive ssRNA genome (46). In contrast, the error rates of DNA replication in eukaryotes and prokaryotes are in the range of 10^{-8}–10^{-11} (47). The polymerase fidelity should set the upper limit for the mutation rate per genome replication *in vivo* (48). The actual mutation rate might be lower as selection pressure *in vivo* will remove unfavorable mutants during replication (49).

To our knowledge, this study presents the first example in the Flaviviridae virus family to characterize the nucleotide incorporation reaction during elongation using transient kinetic methods. The methodology developed here may also be applicable to other polymerases from the Flaviviridae family such as HCV polymerase because of their structural homology (12).

Acknowledgments—We thank Dr. Kenneth Straub and Janice Bleibaum for mass spectrum analysis and Drs. Vincent Leveque and Klaus Klumpp for critical review of the manuscript.

REFERENCES

1. Halstead, S. B. (2007) *Lancet* **370,** 1644–1652
2. Malet, H., Massé, N., Selisko, B., Romette, J. L., Alvarez, K., Guillemot, J. C., Tolou, H., Yap, T. L., Vasudevan, S., Lescar, J., and Canard, B. (2008) *Antiviral Res.* **80,** 23–35
3. Bollati, M., Alvarez, K., Assenberg, R., Baronti, C., Canard, B., Cook, S., Coutard, B., Decroly, E., de Lamballerie, X., Gould, E. A., Grard, G., Grimes, J. M., Hilgenfeld, R., Jansson, A. M., Malet, H., Mancini, E. J., Mastrangelo, E., Mattevi, A., Milani, M., Moureau, G., Neyts, J., Owens, R. J., Ren, J., Selisko, B., Speroni, S., Steuber, H., Stuart, D. I., Unge, T., and Bolognesi, M. (2009) *Antiviral Res.* **87,** 125–148
4. Sampath, A., and Padmanabhan, R. (2009) *Antiviral Res.* **81,** 6–15
5. Beaulieu, P. L. (2010) *Expert. Opin. Ther. Pat.* **19,** 145–164
6. Yap, T. L., Xu, T., Chen, Y. L., Malet, H., Egloff, M. P., Canard, B., Vasudevan, S. G., and Lescar, J. (2007) *J. Virol.* **81,** 4753–4765
7. Selisko, B., Dutartre, H., Guillemot, J. C., Debarnot, C., Benarroch, D., Khromykh, A., Desprès, P., Egloff, M. P., and Canard, B. (2006) *Virology* **351,** 145–158
8. Latour, D. R., Jekle, A., Javanbakht, H., Henningsen, R., Gee, P., Lee, I., Tran, P., Ren, S., Kutach, A. K., Harris, S. F., Wang, S. M., Lok, S. J., Shaw, D., Li, J., Heilek, G., Klumpp, K., Swinney, D. C., and Deval, J. (2010) *Antiviral Res.* **87,** 213–222
9. You, S., and Padmanabhan, R. (1999) *J. Biol. Chem.* **274,** 33714–33722
10. Ackermann, M., and Padmanabhan, R. (2001) *J. Biol. Chem.* **276,** 39926–39937
11. Nomaguchi, M., Ackermann, M., Yon, C., You, S., Padmanabhan, R., and Padmanbhan, R. (2003) *J. Virol.* **77,** 8831–8842
12. Choi, K. H., and Rossmann, M. G. (2009) *Curr. Opin. Struct. Biol.* **19,** 746–751
13. Kapoor, M., Zhang, L., Ramachandra, M., Kusukawa, J., Ebner, K. E., and Padmanabhan, R. (1995) *J. Biol. Chem.* **270,** 19100–19106
14. Villordo, S. M., and Gamarnik, A. V. (2009) *Virus Res.* **139,** 230–239
15. Dutartre, H., Boretto, J., Guillemot, J. C., and Canard, B. (2005) *J. Biol. Chem.* **280,** 6359–6368
16. Cramer, J., Jaeger, J., and Restle, T. (2006) *Biochemistry* **45,** 3610–3619
17. Zhong, W., Uss, A. S., Ferrari, E., Lau, J. Y., and Hong, Z. (2000) *J. Virol.* **74,** 2017–2022
18. Carroll, S. S., Sardana, V., Yang, Z., Jacobs, A. R., Mizenko, C., Hall, D., Hill, L., Zugay-Murphy, J., and Kuo, L. C. (2000) *Biochemistry* **39,**

8243–8249
19. Maag, D., Castro, C., Hong, Z., and Cameron, C. E. (2001) *J. Biol. Chem.* **276,** 46094–46098
20. Lesburg, C. A., Cable, M. B., Ferrari, E., Hong, Z., Mannarino, A. F., and Weber, P. C. (1999) *Nat. Struct. Biol.* **6,** 937–943
21. Malet, H., Egloff, M. P., Selisko, B., Butcher, R. E., Wright, P. J., Roberts, M., Gruez, A., Sulzenbacher, G., Vonrhein, C., Bricogne, G., Mackenzie, J. M., Khromykh, A. A., Davidson, A. D., and Canard, B. (2007) *J. Biol. Chem.* **282,** 10678–10689
22. Choi, K. H., Groarke, J. M., Young, D. C., Kuhn, R. J., Smith, J. L., Pevear, D. C., and Rossmann, M. G. (2004) *Proc. Natl. Acad. Sci. U.S.A.* **101,** 4425–4430
23. Deval, J., D'Abramo, C. M., Zhao, Z., McCormick, S., Coutsinos, D., Hess, S., Kvaratskhelia, M., and Götte, M. (2007) *J. Biol. Chem.* **282,** 16907–16916
24. Ranjith-Kumar, C. T., Kim, Y. C., Gutshall, L., Silverman, C., Khandekar, S., Sarisky, R. T., and Kao, C. C. (2002) *J. Virol.* **76,** 12513–12525
25. Benzaghou, I., Bougie, I., and Bisaillon, M. (2004) *J. Biol. Chem.* **279,** 49755–49761
26. Kati, W. M., Johnson, K. A., Jerva, L. F., and Anderson, K. S. (1992) *J. Biol. Chem.* **267,** 25988–25997
27. Butcher, S. J., Grimes, J. M., Makeyev, E. V., Bamford, D. H., and Stuart, D. I. (2001) *Nature* **410,** 235–240
28. Ferrer-Orta, C., Arias, A., Escarmís, C., and Verdaguer, N. (2006) *Curr. Opin. Struct. Biol.* **16,** 27–34
29. Chinnaswamy, S., Yarbrough, I., Palaninathan, S., Kumar, C. T., Vijayaraghavan, V., Demeler, B., Lemon, S. M., Sacchettini, J. C., and Kao, C. C. (2008) *J. Biol. Chem.* **283,** 20535–20546
30. Hong, Z., Cameron, C. E., Walker, M. P., Castro, C., Yao, N., Lau, J. Y., and Zhong, W. (2001) *Virology* **285,** 6–11
31. Tilton, R. F., Jr., Dewan, J. C., and Petsko, G. A. (1992) *Biochemistry* **31,** 2469–2481
32. Arnold, J. J., and Cameron, C. E. (2004) *Biochemistry* **43,** 5126–5137
33. Arias, A., Arnold, J. J., Sierra, M., Smidansky, E. D., Domingo, E., and Cameron, C. E. (2008) *J. Virol.* **82,** 12346–12355
34. Johnson, K. A. (1993) *Annu. Rev. Biochem.* **62,** 685–713
35. Tsai, Y. C., and Johnson, K. A. (2006) *Biochemistry* **45,** 9675–9687
36. Kellinger, M. W., and Johnson, K. A. (2010) *Proc. Natl. Acad. Sci. U.S.A.* **107,** 7734–7739
37. Lee, H. R., and Johnson, K. A. (2006) *J. Biol. Chem.* **281,** 36236–36240
38. Wong, I., Patel, S. S., and Johnson, K. A. (1991) *Biochemistry* **30,** 526–537
39. Fiala, K. A., and Suo, Z. (2004) *Biochemistry* **43,** 2106–2115
40. Castro, C., Smidansky, E. D., Arnold, J. J., Maksimchuk, K. R., Moustafa, I., Uchida, A., Götte, M., Konigsberg, W., and Cameron, C. E. (2009) *Nat. Struct. Mol. Biol.* **16,** 212–218
41. Ling, H., Boudsocq, F., Woodgate, R., and Yang, W. (2001) *Cell* **107,** 91–102
42. Johnson, A. A., and Johnson, K. A. (2001) *J. Biol. Chem.* **276,** 38090–38096
43. Ahn, J., Werneburg, B. G., and Tsai, M. D. (1997) *Biochemistry* **36,** 1100–1107
44. Johnson, A. A., and Johnson, K. A. (2001) *J. Biol. Chem.* **276,** 38097–38107
45. Donlin, M. J., Patel, S. S., and Johnson, K. A. (1991) *Biochemistry* **30,** 538–546
46. Duffy, S., Shackelton, L. A., and Holmes, E. C. (2008) *Nat. Rev. Genet.* **9,** 267–276
47. Domingo, E., Escarmís, C., Sevilla, N., Moya, A., Elena, S. F., Quer, J., Novella, I. S., and Holland, J. J. (1996) *FASEB J.* **10,** 859–864
48. Castro, C., Arnold, J. J., and Cameron, C. E. (2005) *Virus Res.* **107,** 141–149
49. Mansky, L. M., and Temin, H. M. (1995) *J. Virol.* **69,** 5087–5094